Journal of Materials Chemistry B

ROYAL SOCIETY OF CHEMISTRY

PAPER

View Article Online
View Journal | View Issue

Cite this: J. Mater. Chem. B, 2025, 13, 10009

Biodegradable microneedle-based electrodes for electrophysiological measurements

Sacha Juillard, Anne Planat-Chrétien and Isabelle Texier *

Biopotential recordings such as electroencephalogram (EEG) and electrocardiogram (ECG) generally use wet gel electrodes to ensure a low coupling impedance at the electrode/tissue interface. This set-up is long and tedious and may lead to non-robust signals because of the gel that can leak or dry out. We propose to replace wet gel electrodes with initially dry hydrogel microneedle (MN)-based electrodes capable of piercing the insulating outer layers of the skin and reach the conductive interstitial fluid located in the dermis. Interestingly, purely safe and biodegradable polymer MN tips are able to self-degrade after measurement, increasing safety in the event of microneedle breakage into the skin. We fabricated biocompatible and biodegradable hydrogel-based MN patches made of the cross-linked carboxymethylcellulose (CMC) polymer, rigid and electrically insulating in the dry state, and able to swell once in contact with the ion-conducting interstitial fluid. A metal transduction layer was integrated on the back of the MN patches to obtain the wearable measuring MN-based electrodes. The swelling and ion-conducting capacity of the MN patches were demonstrated. The electrical measurement capability of the MN-based electrodes was assessed using a simple lab-made skin phantom representing the mechanical and electrical properties of the dermis and epidermis. In this proof-of-concept, superior measurement quality was demonstrated with MN-based electrodes in comparison to those of standard wet gel electrodes without any skin preparation. The biodegradable hydrogel-based MN electrodes could therefore offer easy use, patient comfort and safety, and record biopotentials for several hours.

Received 28th March 2025,
Accepted 12th July 2025

DOI: 10.1039/d5tb00727e

rsc.li/materials-b

1. Introduction

Electromyograms (EMGs), electrocardiograms (ECGs), and electroencephalograms (EEGs) are common patient monitoring techniques that rely on the measurement of low frequency (0.5–100 Hz) and low-amplitude (typically few μV for EEG signals) biopotentials. Electrodes commonly used for such recordings must meet several criteria:[1] first, the electrical resistance of the electrodes, skin, and tissue, and the capacitance of the electrode–skin interface, commonly defined as the electrode–skin impedance, must be low (generally less than 10 kΩ at 0.5–100 Hz) to ensure a good signal-to-noise ratio. Second, the electrodes must have a stable behavior with respect to electrode–skin impedance and interfacial chemical reactions to limit measurement drift, noise, and artifacts.

In general, so-called "wet" gel electrodes combining Ag/AgCl electrodes and a conductive gel, most often conveniently pre-coated on the electrodes, are placed on the patient skin. The measurements often require careful preparation of the skin to reduce electrode–skin impedance and promote good contact. This preparation often consists of a combination of shaving the desired sensor location, abrading the skin with sandpaper until it turns red, thoroughly cleaning of the skin with alcohol, ether, or a cleaning gel, and massaging the skin with a conductive gel. This procedure is time-consuming, especially for hairy measurement areas, and may entail a potential risk of infection when abrasion is performed. Furthermore, these electrodes suffer from poor adhesion to the skin, high noise due to sweat and movement, and gradual drying of the gel,[2] which rules out their use for long-term measurements and wearable applications. In addition, due to their application to the superficial layer of the skin (*i.e.* the electrically insulating stratum corneum[3]), they also exhibit sub-optimal signal quality and site-to-site variation,[4] unless thorough cleaning and abrading are performed.

To address these issues, the use of electrically conductive microneedle (MN)-shaped dry electrodes has been proposed.[5–17] Microneedles are typically 400–1500 μm length micro-points able to pierce the stratum corneum and insert in the dermis of the skin. These MN electrodes are generally made of a microneedle-structured substrate made of silicon or steel, or of a polymer subsequently coated with a thin layer of conductive metal. MN electrodes offer excellent measurement quality without prior skin preparation,[9,11,16] especially on hairy skin.[5] Interestingly, MN electrodes set on flexible substrates offer some robustness against movement artifacts,[2,7,8,12] in addition to a reduction in the risk of

Université Grenoble Alpes, CEA, LETI-DTIS, Grenoble, France.
E-mail: isabelle.texier-nogues@cea.fr

detachment and improved patient comfort.[13] As such, they are expected to perform well in long-term electrophysiological monitoring with an increased signal quality compared to non-invasive epidermal sensors whose performances are hampered by the stratum corneum.[18,19]

However, silicon or metal-coated microneedles can raise safety concerns for long-term uses, for example, when worn for several hours per day, such as for home monitoring. Daily movements of the patient can cause a microneedle to break inside the skin, and metallic coating can delaminate. Foreign bodies into the skin can cause discomfort, chronic pain, infections, and neurovascular disorders that may require removal surgery.[20] Therefore, biodegradable microneedles made of soft tissue-like materials once inserted into the skin could present an interesting alternative to mitigate the risks associated with prolonged use and during movements.

Nagamine *et al.* previously proposed for transdermal monitoring a non-swellable (*i.e.* non-hydrogel) MN patch made of a porous methacrylate polymer where the interstitial fluid (ISF) could travel from the tissue through the material pores to contact a hydrogel pad and then a commercial Ag/AgCl electrode.[21] We herein pushed the concept further by fabricating an MN patch with the hydrogel material itself, and coupling it directly to a metallic transducer converting the ionic current into a readable electronic current. Non-soluble crosslinked-hydrogel-based microneedles have been used in the literature as a means to extract interstitial fluid (ISF) for the analysis of biomarkers.[22–25] In the dry state, these devices are able to pierce the rigid outer skin layer, the stratum corneum, then, in contact with the ISF, to swell and absorb the fluid to conduct it towards sensing transducers. The ISF that bathes all tissues and organs displays a composition closely linked to that of blood in terms of ions and metabolites, and therefore presents a high ionic conductivity.[26,27] Therefore, we hypothesized that once swollen with ISF, crosslinked-hydrogel-based microneedles could act as ionic conductors between the tissues and a metallic transducer placed on the back of the MN patch (Fig. 1). Such a device could allow efficient biopotential measurements without skin abrasion, yet overcoming the insulating stratum-corneum skin layer. Advantageously, by selecting a biodegradable hydrogel-based material for the MN patch, the electrode safety would be improved by avoiding metallic layer delamination risk or conductive nanoparticle leaching into the skin during the MN-electrode insertion and retrieval, since in the case of eventual microneedle breaking, it will resorb safely into the tissue. In this paper, we describe a novel MN-based electrode combining a bioresorbable carboxymethyl cellulose-based microneedle patch and a metallic transducer, its characterization, and its performances for electrical measurements using a simple lab-made skin phantom representing the mechanical and electrical properties of the skin.

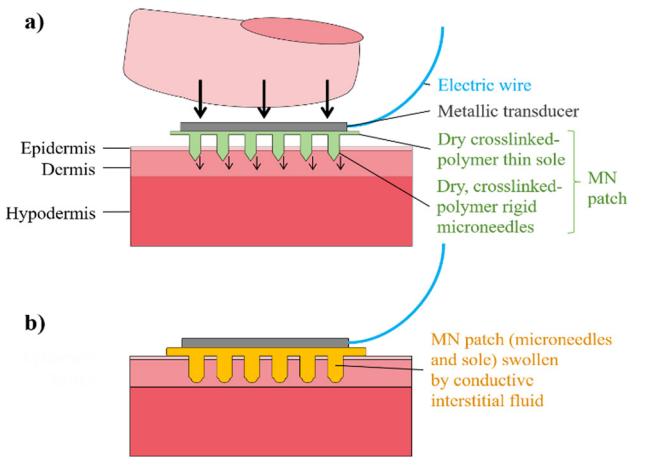

Fig. 1 Concept of crosslinked-hydrogel MN-based electrodes for biopotential measurements. (a) The dry crosslinked polymer cannot mechanically perforate the epidermis and insert the needles into the dermis bathed by the interstitial fluid. (b) The swollen microneedles act as ionic conductors between the tissues and the metallic transducer.

2. Materials and methods

2.1. Preparation and characterization of crosslinked CMC/CA hydrogels

Sodium carboxymethyl cellulose (CMC) (Blanose 7LPEP from Ashland, 90.5 kg mol^{-1}, 0.7 degree of substitution (average number of alcohol functions substituted by carboxymethyl groups on a monomer unit)) was dissolved overnight in distilled water at a concentration of 40 g L^{-1} while stirring. In the standard protocol, citric acid (CA, Sigma-Aldrich) was added with a CO_2H(CA)/OH (CMC) r molar ratio of 0.148 and 0.444. Then, the CMC/CA solution was magnetically stirred for 30 minutes before being poured into Petri dishes (FTIR and swelling measurements) or coated onto glass slides (electrical measurements). The Petri dishes or glass slides were placed in an oven at 30 °C for 24 hours and at 80 °C for 24 hours for complete drying and crosslinking.

Fourier transform infrared (FTIR) absorption spectroscopy was performed on dry crosslinked hydrogels after their demolding from Petri dishes using a Shimadzu MIRacle 10. The spectra were the average of three 80-scan measurements performed from 600 to 4000 cm^{-1} with a 4 cm^{-1} resolution. The hydrogel swelling properties were assessed by weighing the dry materials (m_0) and the materials after different times t of full immersion in PBS at 37 °C (m_t). The percentage of swelling was calculated according to the formula:

$$\text{Percentage of swelling} = (m_t - m_0)/m_0 \times 100.$$

The ability of crosslinked CMC/CA hydrogels to establish an electrical connection between an electrolyte and a metallic transducer was assessed using the experimental set-up depicted in Fig. 3(a). A conductive copper adhesive (Multicomp Pro MP700294, Farnell, France) was set on a 25 mm wide, 75 mm long glass slide, at 35 mm from the bottom of the slide. The CMC/CA solution was cast on the slide and the Cu tape, and then dried as previously described. After drying, a 30 μm thick CMC/CA film was obtained. The glass slide was then held vertically in a large beaker inside which an Ag/AgCl reference electrode was placed at 60 mm from the glass slide. Two wires were connected between a ModuLab XM MTS impedance-meter

(Solartron) and the top end of the Cu tape on one side, and the Ag/AgCl electrode on the other side. The impedance modulus at 10 Hz was recorded as a function of time immediately after filling the beaker with phosphate saline buffer (PBS, 10 mM phosphate, 137 mM NaCl, 2.7 mM KCl, pH 7.4, Sigma-Aldrich) so that 30 mm of the glass slide was submerged and the Cu tape was 5 mm away from the PBS surface.

2.2. Hydrogel microneedle-based electrode fabrication and digital microscopy

Firstly, an aluminum master mold with the desired geometry (18 mm diameter MN patch comprising 137 pencil-shaped 925-μm long microneedles, 850 μm from tip to tip) was fabricated by micromachining. A polydimethylsiloxane (PDMS) mold was then obtained by pouring a degassed PDMS precursor solution with a 10 : 1 precursor : crosslinker mass ratio (Sylgard 184 PDM kit, Sigma-Aldrich), then heating at 100 °C for 1 hour before manual detachment from the aluminum master mold.

600 μL of the CMC/CA solution prepared as previously described were poured into the PDMS molds that were placed in a vacuum chamber at 20 mbar absolute pressure for 5 min, then in an oven at 30 °C for 24 hours and at 80 °C for 24 h. The dry MN patches were manually demolded by gently twisting the PDMS molds. They were placed with their microneedle side down on a soft polyester foam. A 113 mm^2 square or circular metallic transducer, made of an aluminum adhesive tape (3 M, ref. 363, Radio-Spares, France), and connected to an aluminum wire, was gently pressed against the backside of the MN patch to obtain the integrated MN-based electrode.

Digital microscopy images were acquired with a Keyence VHX-7000 digital optical microscope in reflectance mode with ring illumination.

2.3. Fabrication of skin phantom and mechanical characterization

A two-layer skin phantom was developed. The 20 mm thick conductive layer, mimicking the dermis, was a hydrogel composed of gelatin, agar and PBS. 70 g of gelatin (type A, gel strength 300, Sigma-Aldrich) and 2.9 g of agar (Sigma-Aldrich) and eventually 15 mg of neutral red dye (to ease visualization) were dissolved in 290 mL of PBS. The mix was heated in a microwave for 2.5 min at 350 W, energetically stirred with a spatula, and rapidly poured in a 13.6 cm diameter Petri dish. The preparation was gelled overnight under a lid. The electrically insulating epidermis was a 100 μm thick PDMS film obtained by spin-coating a 10 : 1 precursor : crosslinker mass ratio solution (Sylgard 184 PDM kit, Sigma-Aldrich) on the back of a Petri dish and annealing for 1 h at 100 °C. The resulting film was cut to the desired dimensions and placed on top of the freshly prepared dermis-mimicking layer to obtain the complete skin phantom that was kept as much as possible under a lid to prevent drying, and used in the hours following dermis preparation.

Mechanical testing was performed with a TA.XT Plus texturometer (StableMicrosystems). The gelatin-based dermis layer was tested in uniaxial compression with a 28 mm^2 circular probe at 0.4 mm s^{-1} until it reached 75% strain. The PDMS-based epidermis layer was tested as 12 mm wide 19 mm long strips in uniaxial tension at a rate of 0.1 mm s^{-1} until failure. The elastic modulus was calculated as the slope of the stress–strain curves between 0 and 5% strain. Skin phantom's fracture toughness evaluation was performed with an 800 μm diameter conical steel needle (81.2 μm tip with a 15° angle) attached to the uniaxial compression apparatus at 0.01 mm s^{-1}. The toughness was calculated as the integrated area under the force–displacement curve prior to needle insertion, divided by the interfacial needle tip area.

Complete or 4-MN-only MN patches were tested in uniaxial compression with a circular probe of 254 mm^2 (covering the whole MN area) at a speed 0.01 mm s^{-1}. 4-MN patches were obtained by carefully cutting the patches with a sharp blade.

2.4. Impedance and EEG measurements

Impedance measurements (Fig. 3 and 7) were performed using a Palmsens EmStat Pico potentiostat kit (impedance measurements accuracy >99% for $|Z| < 0.1$ GΩ and frequencies < 10 Hz). Measurement sweeps from 100 kHz to 1 Hz (5 points per decade) with a 10-mV alternate voltage perturbation were performed. For skin phantom electrical characterizations (Fig. 7), the testing electrodes (commercial SoftTrace gel electrodes (Conmed Corporation)) were set 2 cm apart.

Simulated EEG-type measurements were performed with the experimental set-up described in Fig. 8(a). "Excitation" was performed with an Agilent® 33250A waveform generator with a 10 dB attenuator. Two commercial SoftTrace gel electrodes (Conmed Corporation) were cut to a diameter of 13 mm yielding a contact area of 133 mm^2, attached on the bottom side of the dermis at 120 mm apart, and connected to the generator. A 10 Hz sinusoidal potential with a 1000 μV amplitude was set through the skin phantom dermis. "Detection" was performed in a two-electrode configuration. The reference was always a SoftTrace gel electrode (contact area of 133 mm^2) set on the dermis layer of the skin phantom. The second test electrode was either a commercial gel electrode set on the dermis (configuration A, Fig. 8) or epidermis (configuration B), or a MN-based electrode inserted into the skin phantom by thumb pressure (configuration C). The test electrodes were placed 120 mm apart from the reference electrode for each configuration. Simulated biopotentials were recorded sequentially on all the electrodes with a commercial EEG recording device from Enobio® (NeuroElectrics). The raw signals were processed according to standard EEG analysis flow with the following filters: notch 50 Hz – butter [0.5–40 Hz].

3. Results and discussion

3.1. Microneedle patch material selection

The material that constituted the electrode MN patch (hydrogel microneedles and sole) had to display high biocompatibility and capability of absorbing ISF, while being mechanically resistant when dry. "Superabsorbent" hydrogels are 3D polymer networks that can absorb up to several times their mass in

water in a few minutes. These hydrogels need to be cross-linked, either physically or chemically, to prevent their rapid dissolution in biological fluids and increase their service time. However, too dense crosslinking can lead to a reduced swelling ability of the hydrogels. We selected carboxymethyl cellulose (CMC) based hydrogels since CMC is a polymer available from renewable resources, acknowledged for its high swelling capability thanks to its carboxylate groups, and considered a safe substance by the United States Federal Drug Administration (FDA).

CMC also possess reactive alcohol and carboxylate functions amenable to form covalent crosslinks to obtain a non-soluble material (Fig. 2(a)).[28–30] We crosslinked the CMC polymer network using citric acid (CA) and mild thermal annealing at 80 °C, forming ester bonds between the carboxylic acid groups (CO_2H) of CA and the alcohol (OH) functions of CMC. Capanema *et al.* reported that the viability of human embryonic kidney cells (HEK293T) was higher than 95% when they come in contact with CMC/CA hydrogels for 24 hours (MTT assay),[28] and Mali *et al.* showed that CMC/CA crosslinked films induced less than 1% hemolysis when in contact with blood.[31] Ester crosslinks are amenable to hydrolysis degradation, stressed in the presence of body fluids by the presence of endogenous esterases. CMC crosslinked hydrogels in general,[32] and therefore CMC/CA materials in particular,[33] are biodegradable, making the hydrogel-based MN biodegradable in the long term in the eventual case of breaking into the tissue.

We used different CO_2H (CA)/OH (CMC) *r* molar ratios (0.148 and 0.444). Note that these molar ratios were calculated taking into account all alcohol and carboxylic acid groups of CMC and CA, all of which cannot react due to steric hindrance. CMC crosslinking was characterized by FTIR spectroscopy. Fig. 2(b) shows the FTIR spectra of CMC, CMC/CA mixtures, and CMC/CA crosslinked hydrogels for r = 0.148 and 0.444, normalized at the 895 cm^{-1} band attributed to the CMC β-1,4 glycoside bond. Characteristics bands of CMC included 3600–3000 cm^{-1} (O–H stretching), 3000–2800 cm^{-1} (C–H stretching), 1593, 1411 and 1319 cm^{-1} (asymmetric and symmetric carboxylate stretching), and 1028 cm^{-1} (C–C–O stretching of primary and secondary alcohol groups). In CMC/CA mixtures, the addition of the carboxylic acid groups of CA was accompanied by a mild acidification of the solution (final pH around 5) and was evidenced by the appearance of two new bands at 1716 and 1242 cm^{-1}, respectively attributed to C=O and C–O stretching of the carboxylic acid groups. Upon hydrogel crosslinking, the esterification reaction was evidenced by the decrease of the OH band at 3600–3000 cm^{-1} as well as those of the carboxylate bands (1593, 1411 and 1319 cm^{-1}), and a small intensity increase at 1716 cm^{-1} and in the region around 1160 cm^{-1}, corresponding respectively to the C=O and C–O stretching bands of the formed ester bonds. These modifications, in agreement with the literature,[28–30] were more pronounced as the r molar ratio increased (Fig. 2).

CMC/CA crosslinking was also confirmed by swelling measurements (Fig. 2c). Without crosslinking (*i.e.* without CA), the dried CMC material swelled immediately and then fully dissolved in 5 minutes when immersed in PBS at 37 °C (no more data in Fig. 2(c) once material is dissolved). In contrast,

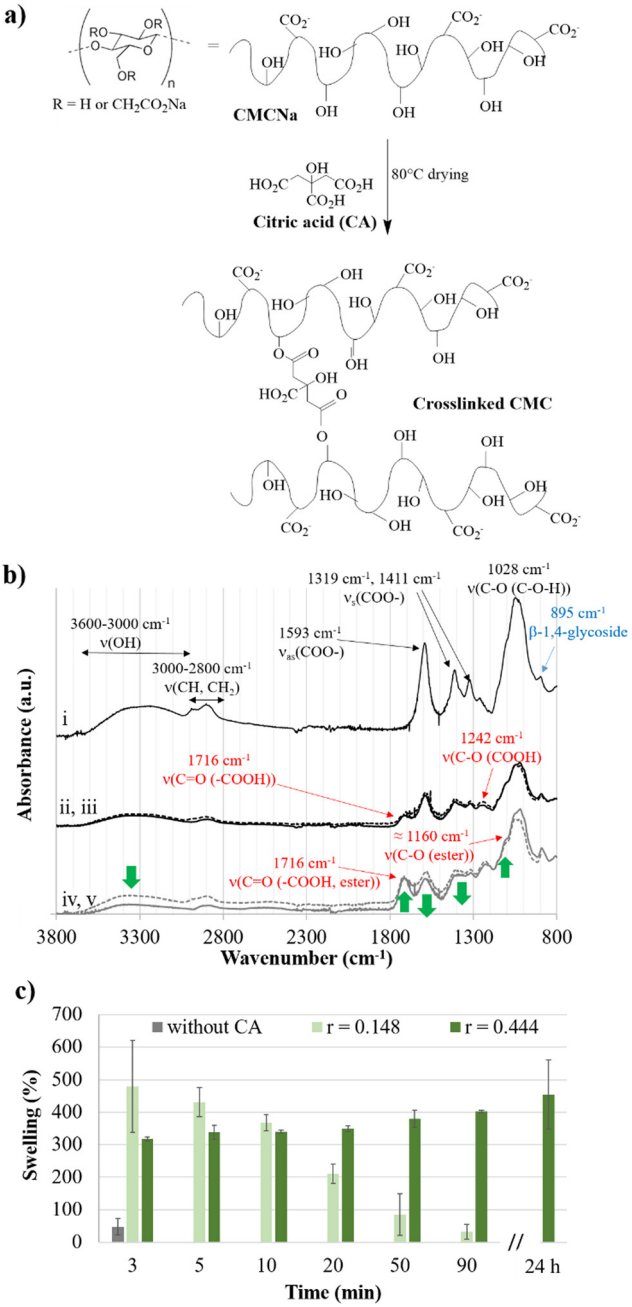

Fig. 2 CMC/CA crosslinking. (a) Reaction scheme. (b) FTIR spectra of CMC (i), CMC/CA mixtures before crosslinking ((ii) and (iv), dashed lines), and crosslinked CMC/CA hydrogels ((iii) and (v), full lines), for different r molar ratios (r = 0.148: (ii) and (iii); r = 0.444: (iv) and (v)). (c) Swelling (%) of CMC and crosslinked CMC/CA materials after immersion in PBS at 37 °C for several durations.

thermally annealed crosslinked CMC/CA materials swelled and remained stable in the gel state with a swelling ratio of about 350% for at least several tens of minutes before dissolving. The more crosslinked the material (the higher the r ratio) was, the slower the material degradation was. It has to be noted that full immersion in PBS, saline and buffered fluid close to physiological conditions, was a more stringent condition for material stability than just the contact of the MN patch tips

with the ISF as expected for MN-electrode insertion in skin. Therefore, we selected the CMC/CA material with r = 0.148 to fabricate the MN patches, since it was expected to represent a good compromise between high swelling capacity and good mechanical properties for self-standing materials, and mid-term biodegradability.

Fig. 3(a) depicts the experimental set-up used to demonstrate the ability of the crosslinked CMC/CA hydrogels to establish the ionic channels between an electrolyte and a metallic transducer. A CMC/CA film was immersed on one side in PBS mimicking the ISF, and connected to another side to a conductive copper tape, the electrical circuit being closed by an Ag/AgCl electrode immersed in the electrolyte. Fig. 3(b) shows the measurement of the impedance modulus at 10 Hz between the Ag/AgCl electrode and the copper tape as a function of time for the CMC/CA r = 0.148 hydrogel. In the initial state, *i.e.* when the CMC film was dry, an impedance modulus of 12 GΩ was measured. This value was equivalent to an open circuit measurement, meaning that the hydrogel was not conductive in the dry state. However, almost immediately after the hydrogel contacted PBS, the impedance drastically dropped to reach 12 kΩ after 6 minutes of immersion. These data highlighted the rapid uptake and travel of conductive PBS through the 5 mm length CMC hydrogel separating the copper tape from the PBS surface. The measured impedance was then stable for at least one hour with an average value of 12.3 kΩ (11.9 to 13.2 kΩ range). Therefore, the CMC/CA hydrogel was confirmed as a promising candidate to design the biodegradable microneedle patch of the device.

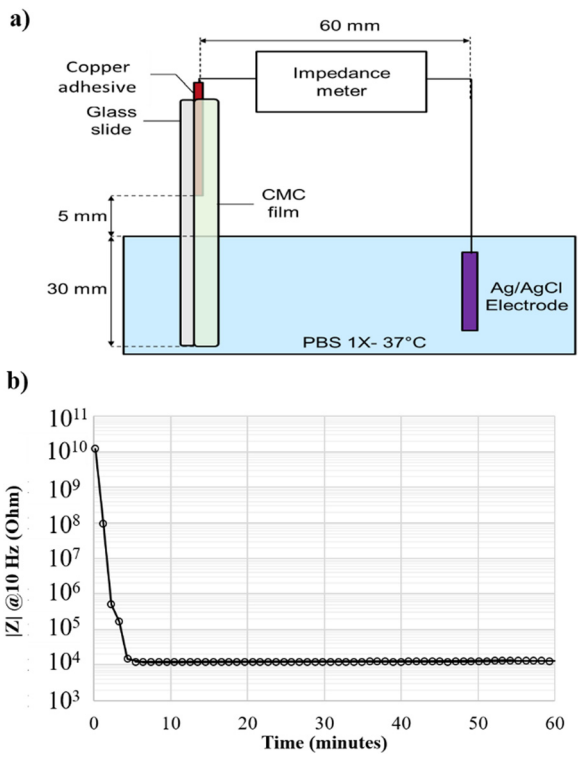

Fig. 3 CMC/CA hydrogel as an electrical bridge. (a) Experiment scheme. (b) Impedance modulus at 10 Hz between the Ag/AgCl electrode and the copper tape as a function of time for CMC/CA r = 0.148 hydrogel.

3.2. Microneedle-based electrode fabrication

The MN-based electrode was obtained by first micro-molding the CMC/CA MN patch, then assembling it with a metallic transducer and electrical wire (Fig. 4). The MN patch aluminum master mold consisted of 137 microneedles evenly distributed with a square pattern on a 12-mm-diameter disk (apparent active area = 113 mm^2) and a 3-mm annular border area without microneedles for ease of handling. The pitch between each microneedle was 850 μm from tip to tip. Each 925-μm long microneedle was shaped like a pencil consisting of a 650-μm-long, 325-μm-diameter shaft and a 275-μm-long tip with a 63° angle. Obtained crosslinked CMC/CA MN patches showed good fidelity to the aluminium master (Fig. 4). In particular, the diameters of the MN tips ranged from 15 to 50 μm, with a median of 20 μm, dimensions acknowledged to allow efficient insertion into the skin.[34–36] A 113 mm^2 metallic transducer and electrical connection wire were then set on the back of the MN patch to obtain the MN-based electrode.

3.3. Mechanical characterization

The mechanical properties of the CMC/CA MN patches were assessed by uniaxial compression tests. Tests performed on complete 137-MN patches showed no visible damage after a 20 N compression. To quantitatively access the MNs yield force F_{yield}, the maximum force applied to the needle before it yields thus preventing its insertion into the skin, and the apparent material elastic modulus E_{app}, MN patches with only the four central MNs (obtained by breaking the others) were tested (Fig. 5). E_{app} was a so-called apparent value because we tested an anisotropic material with a particular geometry, whereas the "true" elastic modulus is a property of an isotropic material. This value represented the amount of force required to deform

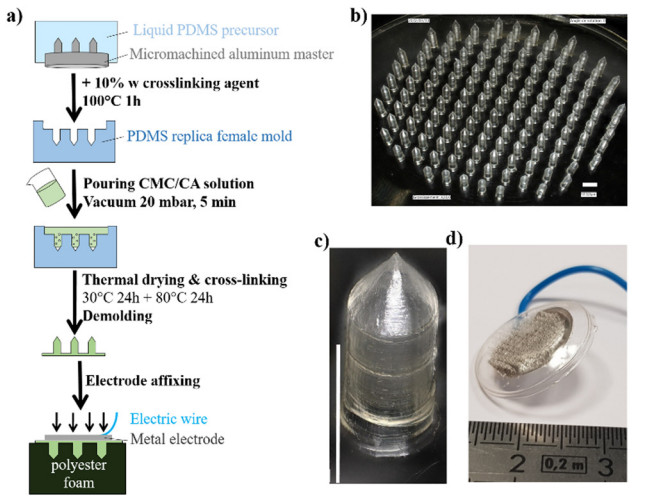

Fig. 4 Fabrication process of the MN-based electrode (a), digital photographs of the CMC/CA MN patch (b) and a microneedle (c), and photograph of the integrated electrode (d). Scale bar for (b) and (c): 500 μm.

elastically the MNs (*i.e.* in the linear portion of the force–displacement curve, Fig. 5). This elastic regime (region A) where the microneedles deformed elastically, *i.e.* without suffering permanent damage, extended from 0 to 30 μm with E_{app} = 0.027 ± 0.006 N μm^{-1} for four MNs. In region B (30 to 50 μm displacement), the curve deviated from linearity, showing a viscoelastic behaviour of crosslinked CMC. In region C, the force dramatically decreased due to the needle yield. The critical force F_{yield} was measured as 1.3 ± 0.4 N for four MNs. This decrease was not sharp, demonstrating the ductile nature of the material.

F_{yield} and E_{app} are known to increase linearly with the contact area between the MNs and the skin.[37,38] Therefore, assuming an identical microneedle geometry throughout the patch and a flat sole, these parameters also scale linearly with the number of MNs. For a full MN patch with 137 microneedles, we calculated F_{yield} = 43 ± 11 N and E_{app} = 0.94 ± 0.18 N μm^{-1}. The literature reports insertion forces ranging from a few Newtons to 30 N in human or porcine skin, for MN patches with a similar tip radius and number of MNs than those used in this study.[35–37,39,40] Therefore, we expected the MN patches to insert successfully into human skin with a negligible microneedle deformation (28 μm for a 30 N insertion force).

3.4. Design of skin phantom for MN-based electrode functional characterization

In order to avoid systematic *in vivo* testing of medical devices during development, *ex vivo* skin samples or so called "phantoms" mimicking tissue relevant properties are required. In our case, we needed to dispose of a tissue model with a dry insulating surface for the top of the skin, and a hydrated layer representing the dermis bathed by the ISF fluid with a suitable water content. Unfortunately, *ex vivo* porcine skin samples could not fulfill these constraints of dry surface while presenting a hydrated dermis layer, and dried too quickly to be properly handled for the proof-of-concept of the hydrogel MN-based electrodes. Therefore, we turned ourselves towards the design of a representative skin phantom fulfilling our needs, and the following specifications. First, the surface of the phantom, representing the epidermis, had to be dry and display a high electrical resistivity and a thickness representative of that of the epidermis layer (typically several tens of kΩ for dehydrated skin,[27,41,42] and about 80–100 μm,[43] respectively). Second, the inner layer of the skin phantom, representing the dermis and hypodermis, where the MNs should insert, was expected to contain a representative content of the electrolyte fluid with a conductivity similar to that of the ISF (75–80% fluid content in skin, with ISF typical conductivity values of 5–20 mS cm^{-1} (ref. 27)). Third, the mechanical properties of the skin phantom had to be consistent with those of the skin to some extent.

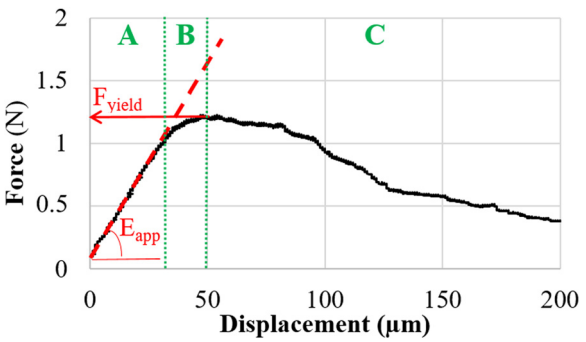

Fig. 5 Uniaxial compression test of a four microneedles patch. Domains A–C are delimitated as shown in green. The red arrow points to the graphical reading of the yield force, and the dashed red line indicates the linear elastic deformation region where the slope is the apparent elastic modulus E_{app}.

To meet these specifications, a two-layer skin phantom was developed. A 20 mm thick conductive layer composed of a gelatin : agar : PBS buffer (19.2 : 0.8 : 80 weight ratio) hydrogel was used to mimic the conductive and mechanical properties of the dermis. PBS displays an ionic composition and conductivity (15–20 mS cm^{-1}) close to those of ISF.[27] Similar gelatin/agar phantoms were previously acknowledged as mimicking the mechanical properties of the dermis.[44] A wide range of dermis elastic moduli, from 10 to 1610 kPa,[45–47] are reported in the literature, depending on the test location and local orientation of the collagen fibers, and the testing method (*e.g.* scale of measurement, size of the probe, and experiment design).[48] We performed compression tests to evaluate the mechanical behavior of our phantom dermis (Fig. 6(a)). The dermis layer showed a mostly elastic, *i.e.* linear, behavior until about 40% strain, with a measured elastic modulus of 400 ± 30 kPa (0–5% strain), that laid in the literature-reported values for dermis. The insulating and dry stratum corneum was modeled by a 93-μm-thick hydrophobic non-porous silicone dry film that was mechanically characterized by tensile tests (Fig. 6(b)). The epidermis layer demonstrated resistance to stretch until about 70% strain, with a measured tensile elastic modulus of 1 ± 0.2 MPa in the 0–5% strain range. This value was consistent with the elastic moduli of the epidermis layer reported in the literature, ranging from 0.60 to 1000 MPa.[45,49]

The two layers were then assembled to produce what is referred to as a complete skin phantom. The wet dermis layer promoted sufficient adhesion with the epidermis layer to avoid its delamination during use. A needle is assumed to be inserted into the skin once the energy delivered by the needle on the tissue surpasses its fracture energy, also referred to as the fracture toughness.[37] Therefore, a steel needle was used to measure the skin phantom toughness in a piercing test (Fig. 6(c)). A sharp force drop was observed between 1800 and 2050 μm needle displacement. This occurred when the steel needle pierced through the rigid silicone (epidermis) layer and reached the dermis layer. The fracture toughness, defined as the integrated area below the force–displacement curve divided by the area of the needle tip (81.2 μm diameter) was 52 ± 3 kJ m^{-2}. The literature reports toughness of the human abdomen skin in the range of 20–30 kJ m^{-2}.[37,38] Therefore, our skin phantom appeared about 2-fold harder to pierce than the abdomen skin. Yet, it was fully relevant to demonstrate the capacity of the MN-electrode to pierce human skin.

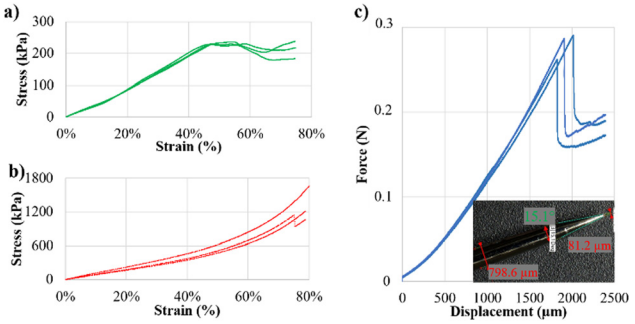

Fig. 6 Mechanical characterization of skin phantom. (a) Compression measurements performed on the gelatin:agar:PBS dermis layer (measurements on 3 independent materials). (b) Tensile measurements performed on the silicone epidermis layer (measurement on 3 independent materials). (c) Force–displacement curves during the insertion of a steel needle (photograph in inset) in a complete skin phantom (measurement on 3 independent materials).

The electrical properties of the skin phantom were assessed with commercial gel electrodes using the experimental set-up described in Fig. 7. In configuration A, where the two electrodes are set on the dermis layer, we checked the electrical conductivity of the dermis. An initial impedance of 0.14 kΩ cm^2 was measured, slightly increasing to 0.28 kΩ cm^2 after 16 hours of use. This slight increase was attributed to the gradual drying of the phantom with time. In configuration B, where one electrode laid on the dermis and the other on the full skin phantom, we checked the insulating properties of the epidermis layer. The measured initial impedance was 0.13 GΩ cm^2 increasing to 0.17 GΩ cm^2 in 2 hours. This value was very high compared to a measurement on human skin (several tens of kΩ).[41,42] However, the present model was highly relevant to provide the validation that the MN hydrogel patch allowed electrical connection between the fluid-rich dermis layer and the metallic transducer of the device through an insulating epidermis.

3.5. Induced dynamic electrophysiological signal measurement on skin phantom

Acquisition of simulated biopotentials was investigated with the setup displayed in Fig. 8(a). This setup consisted of two parts. The first one labelled "Excitation" in the diagram, devoted to electrical excitation, consisted of two electrodes attached to the conductive (dermis) bottom side of the skin phantom and were connected to a potential waveform generator. A 10 Hz sinusoidal potential with a 1000 μV amplitude was then applied through the dermis of the skin phantom. The second part labelled "Detection" in the diagram consisted in an EEG measurement set-up with a reference electrode (commercial gel electrode) placed onto the conductive dermis and a measurement electrode. Three different configurations of measurement electrodes placed at the same distance (120 mm) from the reference were tested. Configuration A used a commercial gel electrode placed directly on the conductive dermis. It represented a measurement on prepared and abraded skin. Configuration B tested a commercial gel electrode placed on the insulating 100 μm thick epidermis. It represented a measurement on unprepared skin. Configuration C tested our MN-based electrode inserted into the skin layers through the epidermis without any previous skin abrasion.

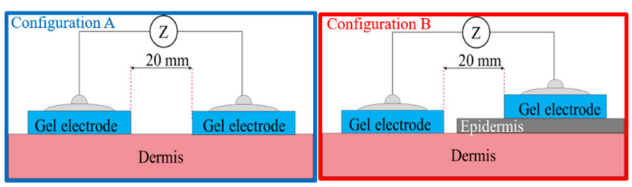

Fig. 7 Experimental set-up to characterize the electrical skin phantom properties.

Fig. 8(b) shows the 10 Hz impedance measurements obtained for 100 minutes with the different configurations. Whereas impedance signals were stable with time for configurations A and B (commercial gel electrodes) laid respectively onto the conductive dermis and the insulating epidermis, the impedance signal decreased with time for the MN-electrode (configuration C). Electrode A displayed a mean impedance of 252 Ω, and recorded a sinusoidal signal of 167 μV amplitude at all times between 0 and 100 minutes of recording (Fig. 8(c)). This measurement represented good EEG measuring conditions but required skin peeling of the stratum corneum (*i.e.*, removing the insulating epidermis layer) before the experiment. Conversely, electrode B measured an impedance of 0.1 GΩ and was not able to record a sinusoidal signal (maximum amplitude of ±5 μV, limit of detection) due to the insulating skin phantom epidermis (Fig. 8(d)). This configuration with measurement on dry skin without abrasion resulted in very poor EEG-type measuring conditions.

Configuration C tested an MN electrode inserted into the skin layers through the 100 μm thick epidermis. A few seconds after insertion, *i.e.*, before the CMC hydrogel swelled with conductive fluid, the dry microneedles behaved as an electrical insulator ($|Z|$ = 745 kΩ) (Fig. 8b). A noisy, low amplitude signal was recorded with poor agreement with the input sinusoidal pattern (Fig. 8(e)–(i)). As time passed and fluid swelled into the MN patch, the impedance decreased dramatically, and the recorded signal amplitude and the agreement with the sinus shape increased (Fig. 8e). 31 minutes after insertion, a sinusoidal signal of 103 μV amplitude with $|Z|$ = 12 kΩ was obtained. On a longer time scale, the impedance continued to slightly decrease for 16 hours (−1.2% at 16 hours compared to 100 minutes), indicating that the wet dermis layer continued to maintain the CMC microneedle patch in a swollen state, favourable to prolonged measurements.

The sensitivity and limit of detection of the MN-based electrodes were also investigated by plotting the measured signal amplitude in configuration C (MN device on intact skin) compared to configuration A (commercial gel electrode on abrased skin) for a thicker epidermis layer (about 300 μm) (Fig. 9). The linearity of the measured signal amplitude with the input voltage amplitude was verified in both configurations. The limit of detection was about 5 μV. The achieved sensitivity for configuration C was about 2/3 of that of configuration A.

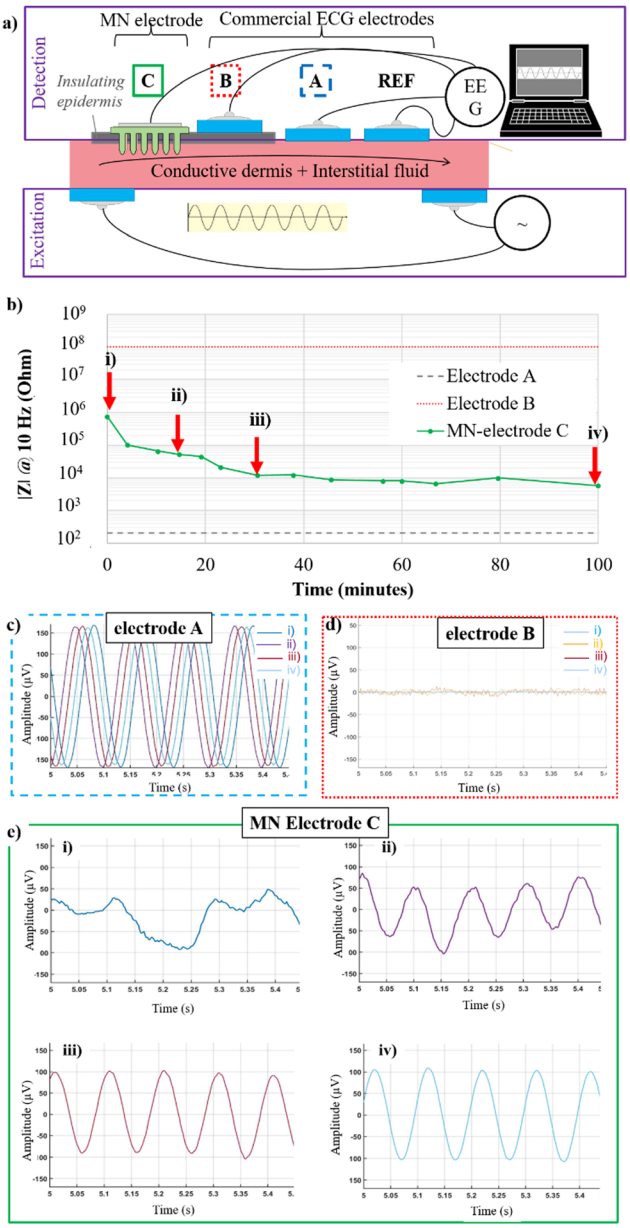

Fig. 8 Dynamic electrophysiological signal measurements on skin phantom. (a) Setup used to input on the bottom side and detect on the top side a sinusoidal potential through the skin phantom. (b) Impedance modulus measured at 10 Hz for the three different configurations A–C. Four points (i)–(iv) are labeled where potential recording are shown in (c)–(e). (c)–(e) Sinusoidal pattern acquired for configuration A (c), B (d), and C (e) at the four recording times ((i) insertion time, (ii) 15 min, (iii) 31 min, (iv) 100 min after insertion).

The ability of the MN-based electrode to perforate the skin was assessed by digital microscopy (Fig. 10). The analysis of the epidermis layer, once separated from the MN-patch and the dermis layer was not clear. No clear signs of perforation could be evidenced on this phantom layer, due to poor optical contrast and traces of swollen hydrogels originating from both the dermis and the MN patch. However, the analysis of the dermis layer evidenced clearly the microneedle pattern of the MN patch (Fig. 10(a)). Additionally, the swelling of the hydrogel

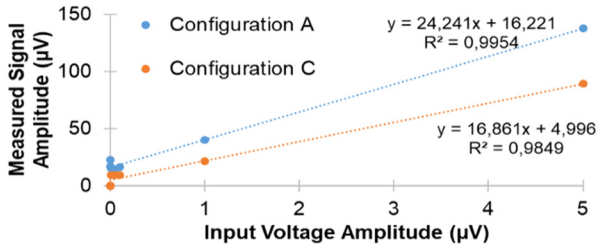

Fig. 9 Measured signal amplitude *versus* input signal amplitude for measurements performed in configurations A and C of Fig. 7(a).

MN-electrode after one hour insertion into the skin phantom was clearly evidenced (Fig. 10(b)), demonstrating that the MN tips had reached the dermis layer through the impermeable epidermis, and were able to convey the fluid into the whole MN patch. It was not possible to withdraw and weight the MN-electrode device for precise quantification of fluid uptake with time after insertion into the skin phantom, since after insertion, the MN patch could not be properly separated from the epidermis silicon layer. However, qualitative visual observation showed that the hydrogel MN patch reached swelling equilibrium within 40–60 minutes after phantom insertion. Notably, the swelling of the hydrogel MN patch was far slower than what was observed for the full immersion of the material (a few minutes, Fig. 2(c)), due to the reduced surface area of the device (only MN tips) that is in contact with the fluid. To note that if the initially dried material transformed into a "humid" hydrogel material, geometrical change of the patch on top of the skin phantom was moderate (<10% diameter increase). After 16 hours of insertion of the device, no significant change was observed in the visual aspect of the hydrogel MN patch, which looked similar to what was observed after 1 hour of insertion.

Interestingly, the qualitative observation of the microneedle patch reaching swelling equilibrium within 40–60 minutes after phantom insertion was correlated with the obtention of the impedance plateau obtained in about 40 minutes after insertion (Fig. 8(b)). This strengthens the idea that the progressive hydration of the CMC/CA material created an increasing number of pathways for the ionic fluid to travel through the cross-linked polymer network and establish electrical contact with

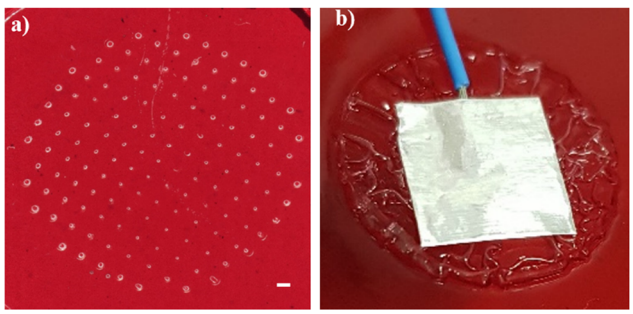

Fig. 10 MN perforation assessment by digital microscopy. (a) Digital microscopy image of the dermis layer after removal of the MN-electrode and the epidermis layer. (b) Photograph of the MN device after 1 hour of insertion in the skin phantom. Scale bar: 500 μm.

the electrode inserted on the back of the device. The shape of the sinusoidal electrical signal indeed improved during this lapse of time (Fig. 8(e)), indicating that measurement accuracy and signal stability were progressively improved during material swelling.

All these results demonstrated that the hydrogel microneedle-based electrodes are promising candidates to ensure the coupling between an EEG sensor and the biological tissues. The initially dry hydrogel microneedles, becoming wet *in situ*, allowed the detection of low-frequency signals without the need for skin preparation and without the disadvantages of the separate use of a gel.

4. Conclusions

An electrode for biopotential measurements (EEG–ECG–EMG-like) based on a biodegradable polymeric microneedle patch was designed and easily manufactured by a simple polymer moulding process. A skin phantom capable of mimicking some mechanical and electrical properties of the dermis and epidermis was developed to establish the proof of concept of the MN-based electrode. We showed that the biopolymer-based MN electrode could record, without any skin preparation (*i.e.*, epidermis removal), simulated biopotentials for several hours, unlike conventional electrodes, which require a skin preparation step and the use of a gel to ensure electrical coupling. This proof of concept paves the way for further optimizations. This includes a further study of the materials to obtain the best compromise between the mechanical properties of the hydrogel (allowing dry perforation), the swelling properties, and its degradability. The performance of the microneedle electrode as an electrical coupling interface could also be further optimized in terms of surface density (number of microneedles per cm^2), surface area, and geometry of the microneedle itself.

Conventional electrodes are quite time-consuming to install and, after prolonged examination, the coupling, due to drying and/or spreading of the gel, can be modified, disturbing the signal recording. Here, we have demonstrated the potential of the hydrogel-based microneedle electrodes for safe and relatively long-term measurements. Advantageously, these devices are also very easy to fabricate by a low-cost process using a polymer, CMC, derived from renewable resources.

Author contributions

Sacha Juillard: data curation, investigation, methodology, visualization, and writing – original draft. Anne Planat-Chrétien: conceptualization, funding acquisition, methodology, supervision, and writing – original draft. Isabelle Texier: conceptualization, funding acquisition, methodology, supervision, and writing – original draft.

Conflicts of interest

There are no conflicts to declare.

Data availability

Due to CEA-LETI legal confidentiality requirements, data will be made available on request.

Acknowledgements

The authors greatly acknowledge the help of Manuel Alessio, Aminata Diarra, and Nicolas Verplanck for the design and fabrication of the aluminum master molds. This work was funded by the French National Research Agency in the framework of the LETI Carnot program (MN4MMD project). LETI-DTIS is supported by the French National Research Agency in the framework of the Labex Arcane, CBH-EUR-GS program (ANR-17-EURE-003) and Glyco@Alps ''Investissement d'Avenir'' program (ANR-15-IDEX-02).

References

1 G. A. Light, L. E. Williams, F. Minow, J. Sprock, A. Rissling, R. Sharp, N. R. Swerdlow and D. L. Braff, Electroencephalography (EEG) and Event-Related Potentials (ERPs) with Human Participants, *Curr. Protoc. Neurosci.*, 2010, **52**, 6.25.21–26.25.24.

2 M. Kim, T. Kim, D. S. Kim and W. K. Chung, Curved Microneedle Array-Based sEMG Electrode for Robust Long-Term Measurements and High Selectivity, *Sensors*, 2015, **15**, 16265–16280.

3 D. Miklavčič, N. Pavšelj and F. X. Hart, Electric Properties of Tissues, *Wiley Encyclopedia of Biomedical Engineering*, 2006, DOI: **10.1002/9780471740360.ebs0403**.

4 N. A. Alba, R. J. Sclabassi, M. Sun and X. T. Cui, Novel Hydrogel-Based Preparation-Free EEG Electrode, *IEEE Trans. Neural Syst. Rehabil. Eng.*, 2010, **18**, 415–423.

5 M. Arai, Y. Kudo and N. Miki, Polymer-based candle-shaped microneedle electrodes for electroencephalography on hairy skin, *Jpn. J. Appl. Phys.*, 2016, **55**, 06GP16.

6 C. Dong, L. Tran, T. Q. Nguyen and W. T. Park, Microneedle electrodes for bio-potential health monitoring, *JMST Adv.*, 2024, **6**, 227–232.

7 Y. Hou, Z. Li, Z. Wang and H. Yu, Miura-ori structured flexible microneedle array electrode for biosignal recording, *Microsyst. Nanoeng.*, 2021, **7**, 53.

8 J. Li, Y. Ma, D. Huang, Z. Wang, Z. Zhang, Y. Ren, M. Hong, Y. Chen, T. Li, X. Shi, L. Cao, J. Zhang, B. Jiao, J. Liu, H. Sun and Z. Li, High-Performance Flexible Microneedle Arrayas a Low-Impedance Surface Biopotential DryElectrode for Wearable Electrophysiological Recording and Polysomnography, *Nano-Micro Lett.*, 2022, **14**, 132.

9 J. Lozano and B. Stoeber, Fabrication and characterization of a microneedle array electrode with flexible backing for biosignal monitoring, *Biomed. Microdev.*, 2021, **23**(4), 53.

10 P. R. Miller, R. J. Narayan and R. Polsky, Microneedle-based sensors for medical diagnosis, *J. Mater. Chem. B*, 2016, **4**, 1379–1383.

11 C. O'Mahony, K. Grygoryev, A. Ciarlone, G. Giannoni, A. Kenthao and P. Galvin, Design, fabrication and skin-electrode contact analysis of polymer microneedle-based ECG electrodes, *J. Micromech. Microeng.*, 2016, **26**, 084005.
12 W. Pei, H. Zhang, Y. Wang, X. Guo, X. Xing, Y. Huang, Y. Xie, X. Yang and H. Chen, Skin-potential Variation Insensitive Dry Electrodes for ECG Recording, *IEEE Trans. Biomed. Eng.*, 2017, **64**, 463–470.
13 M. Rajabi, N. Roxhed, R. Z. Shafagh, T. Haraldson, A. C. Fischer, W. V. D. Wijngaart, G. Stemme and F. Niklaus, Flexible and Stretchable Microneedle Patches with Integrated Rigid Stainless Steel Microneedles for Transdermal Biointerfacing, *PLoS One*, 2016, **11**, e0166330.
14 G. Stavrinidis, K. Michelakis, V. Kontomitrou, G. Giannakakis, M. Sevrisarianos, G. Sevrisarianos, N. Chaniotakis, Y. Alifragis and G. Konstantinidis, SU-8 microneedles based dry electrodes for Electroencephalogram, *Microelectron. Eng.*, 2016, **159**, 114–120.
15 R. Wang, J. Bai, X. Zhu, Z. Li, L. Cheng, G. Zhang and W. Zhang, A PDMS-based microneedle array electrode for long-term ECG recording, *Biomed. Microdev.*, 2022, **24**, 27.
16 R. Wang, X. Jiang, W. Wang and Z. Li, A microneedle electrode array on flexible substrate for long-term EEG monitoring, *Sens. Actuators, B*, 2017, **244**, 750–758.
17 W. Zhou, R. Song, X. Pan, Y. Peng, X. Qi, J. Peng, K. S. Hui and K. N. Hui, Fabrication and impedance measurement of novel metal dry bioelectrode, *Sens. Actuators, A*, 2013, **201**, 127–133.
18 S. Choi, H. Lee, R. Ghaffari, T. Hyeon and D.-H. Kim, Recent Advances in Flexible and Stretchable Bio-ElectronicDevices Integrated with Nanomaterials, *Adv. Mater.*, 2016, **28**, 4203–4218.
19 S. Yang, Y.-C. Chen, L. Nicolini, P. Pasupathy, J. Sacks, B. Su, R. Yang, D. Sanchez, Y.-F. Chang, P. Wang, D. Schnyer, D. Neikirk and N. Lu, Cut-and-Paste Manufacture of Multiparametric Epidermal Sensor Systems, *Adv. Mater.*, 2015, **27**, 6423–6430.
20 J. Rupert, J. D. Honeycutt and M. R. Odom, Foreign Bodies in the Skin: Evaluation and Management, *Am. Fam. Physician*, 2020, **101**, 740–747.
21 K. Nagamine, J. Kubota, H. Kai, Y. Ono and M. Nishizawa, An array of porous microneedles for transdermal monitoring of intercellular swelling, *Biomed. Microdev.*, 2017, **19**, 68.
22 A. Caliò, P. Dardano, V. Di Palma, M. F. Bevilacqua, A. Di Matteo, H. Iuele and L. De Stefano, Polymeric microneedles based enzymatic electrodes for electrochemical biosensing of glucose and lactic acid, *Sens. Actuators, B*, 2016, **236**, 343–349.
23 P. G. Nejad, A. G. Nejad, H. Zheng, K. Dhingra, M. Samarikhalaj and M. Poudineh, A Conductive Hydrogel Microneedle-Based Assay Integrating PEDOT:PSS and Ag-Pt Nanoparticles for Real-time, Enzyme-less, and Electrochemical Sensing of Glucose, *Adv. Healthcare Mater.*, 2023, **12**, 2202362.
24 M. Zheng, Z. Wang, H. Chang, L. Wang, S. W. T. Chew, D. C. S. Lio, M. Cui, L. Liu, B. C. K. Tee and C. Xu, Osmosis-Powered Hydrogel Microneedles for Microliters of Skin Interstitial Fluid Extraction within Minutes, *Adv. Healthcare Mater.*, 2020, **9**, 1901683.
25 B. Darmau, M. Sacchi, I. Texier and A. J. Gross, Self-Extracting Dextran-Based Hydrogel Microneedle Arrays with an Interpenetrating Bioelectrocatalytic Sensor for Transdermal Monitoring with Matrix Protection, *Adv. Healthcare Mater.*, 2025, **14**, 2403209.
26 K. F. Dobiszewski, M. P. Deek, A. Ghaly, C. Prodan and A. A. Hill, Extracellular fluid conductivity analysis by dielectric spectroscopy for in vitro determination of cortical tissue vitality, *Physiol. Meas.*, 2012, **33**, 1249–1260.
27 M. J. Peters, J. G. Stinstra and I. Leveles, in *Modeling and Imaging of Bioelectrical Activity: Principles and Applications*, ed. B. He, Springer US, Boston, MA, 2005, pp. 281–319.
28 N. S. V. Capanema, A. A. P. Mansur, A. C. de Jesus, S. M. Carvalho, L. C. de Oliveira and H. S. Mansur, Superabsorbent crosslinked carboxymethyl cellulose-PEG hydrogels for potential wound dressing applications, *Int. J. Biol. Macromol.*, 2018, **106**, 1218–1234.
29 C. Demitri, R. D. Sole, F. Scalera, A. Sannino, G. Vasapollo, A. Maffezzoli, L. Ambrosio and L. Nicolais, Novel superabsorbent cellulose-based hydrogels crosslinked with citric acid, *J. Appl. Polym. Sci.*, 2008, **110**, 2453–2460.
30 S. H. Aswathy, U. NarendraKumar and I. Manjubala, Physicochemical Properties of Cellulose-Based Hydrogel for Biomedical Applications, *Polymers*, 2022, **14**, 4669.
31 K. K. Mali, S. C. Dhawale, R. J. Dias, N. S. Dhane and V. S. Ghorpade, Citric Acid Crosslinked Carboxymethyl Cellulose-based Composite Hydrogel Films for Drug Delivery, *Indian J. Pharm. Sci.*, 2018, **80**, 657–667.
32 W. Zhang, Y. Liu, Y. Xuan and S. Zhang, Synthesis and Applications of Carboxymethyl Cellulose Hydrogels, *Gels*, 2022, **8**, 529.
33 N. M. Kanafi, N. A. Rahman and N. H. Rosdi, Citric acid cross-linking of highly porous carboxymethyl cellulose/poly(ethylene oxide) composite hydrogel films for controlled release applications, *Mater. Today: Proc.*, 2019, **7**, 721–731.
34 J. Kim, S. Park, G. Nam, Y. Choi, S. Woo and S.-H. Yoon, Bioinspired microneedle insertion for deep and precise skin penetration with low force: Why the application of mechanophysical stimuli should be considered, *J. Mech. Behav. Biomed. Mater.*, 2018, **78**, 480–490.
35 A. Ripolin, J. Quinn, E. Larrañeta, E. M. Vicente-Perez, J. Barry and R. F. Donnelly, Successful application of large microneedle patches by human volunteers, *Int. J. Pharm.*, 2017, **521**, 92–101.
36 A. M. Römgens, D. L. Bader, J. A. Bouwstra, F. P. T. Baaijens and C. W. J. Oomens, Monitoring the penetration process of single microneedles with varying tip diameters, *J. Mech. Behav. Biomed. Mater.*, 2014, **40**, 397–405.
37 S. P. Davis, B. J. Landis, Z. H. Adams, M. G. Allen and M. R. Prausnitz, Insertion of microneedles into skin: measurement and prediction of insertion force and needle fracture force, *J. Biomech.*, 2003, **37**, 1155–1163.
38 P. Khanna, K. Luongo, J. A. Strom and S. Bhansali, Sharpening of hollow silicon microneedles to reduce skin penetration force, *J. Micromech. Microeng.*, 2010, **20**, 045011.

39 R. F. Donnelly, M. J. Garland, D. I. J. Morrow, K. Migalska, T. R. R. Singh, R. Majithiya and A. D. Woolfson, Optical coherence tomography is a valuable tool in the study of the effects of microneedle geometry on skin penetration characteristics and in-skin dissolution, *J. Controlled Release*, 2010, **147**, 333–341.

40 E. Larrañeta, J. Moore, E. M. Vicente-Pérez, P. González-Vázquez, R. Lutton, A. D. Woolfson and R. F. Donnelly, A proposed model membrane and test method for microneedle insertion studies, *Int. J. Pharm.*, 2014, **472**, 65–73.

41 T. Yamamoto and Y. Yamarnoto, Electrical properties of the epidermal stratum corneum, *Med. Biol. Eng.*, 1976, **14**, 151–158.

42 Y. Yamamoto, T. Yamamoto and T. Ozawa, Characteristics of skin admittance for dry electrodes and the measurement of skin moisturization, *Med. Biol. Eng. Comput.*, 1986, **24**, 71–77.

43 D. A. Lintzeri, N. Karimian, U. Blume-Peytavi and J. Kottner, Epidermal thickness in healthy humans: a systematic review and meta-analysis, *J. Eur. Acad. Dermatol. Venereol.*, 2022, **36**, 1191–1200.

44 A. I. Chen, M. L. Balter, M. I. Chen, D. Gross, S. K. Alam, T. J. Maguire and M. L. Yarmush, Multilayered tissue mimicking skin and vessel phantoms with tunable mechanical, optical, and acoustic properties, *Med. Phys.*, 2016, **43**, 3117–3131.

45 M. F. Leyva-Mendivil, A. Page, N. W. Bressloff and G. Limbert, A mechanistic insight into the mechanical role of the stratum corneum during stretching and compression of the skin, *J. Mech. Behav. Biomed. Mater.*, 2015, **49**, 197–219.

46 A. Delalleau, G. Josse, J.-M. Lagarde, H. Zahouani and J.-M. Bergheau, A nonlinear elastic behavior to identify the mechanical parameters of human skin in vivo, *Sking Res. Technol.*, 2008, **14**, 152–164.

47 A. Delalleau, G. Josse, J.-M. Lagarde, H. Zahouani and J.-M. Bergheau, Characterization of the mechanical properties of skin by inverse analysis combined with the indentation test, *J. Biomech.*, 2006, **39**, 1603–1610.

48 J. van Kuilenburg, M. A. Masen and E. van der Heide, Contact modelling of human skin: What value to use for the modulus of elasticity?, *Proc. Inst. Mech. Eng., Part J.*, 2013, **227**, 349–361.

49 M. L. Crichton, X. Chen, H. Huang and M. A. F. Kendall, Elastic modulus and viscoelastic properties of full thickness skin characterised at micro scales, *Biomaterials*, 2013, **34**, 2087–2097.